Inorg. Chem. **2004**, *43*, 1388–1394

Axial Ligand Exchange in Chiral Macrocyclic Ytterbium(III) Complexes

Jerzy Lisowski,*,† Silvia Ripoli,‡ and Lorenzo Di Bari*,‡

Dipartimento di Chimica e Chimica Industriale, Università di Pisa, via Risorgimento 35, 56126 Pisa, Italy, and Department of Chemistry, University of Wrocław, F. Joliot-Curie 14, 50383 Wrocław, Poland

Received December 3, 2003

We investigate the role of axial ligands on the near-IR-optical and paramagnetic NMR spectra of the complex $[Yb\mathbf{L}]^{+3}$ where **L** is the stereodefined enantiopure chiral macrocycle (**L** = hexaazapentacyclo[25.3.1.1^{12,24}.0^{4,9}.0^{19,24}]-dotriaconta-1(31),2,10,12,14,16(32),17,25,27,29-decaene). The conformation in solution of the lanthanide complex is characterized by analyzing the pseudocontact ^{1}H NMR shifts and is consistent with X-ray data of single crystal of analogue systems. The macrocycle is confined within a thin equatorial disk, leaving the cation open to at least two axial sites, on the opposite hemispheres. We recorded, assigned, and analyzed the ^{1}H NMR spectra of several species upon changing the anion in solution, calculating the magnetic susceptibility anisotropy tensor for each. Near-IR circular dichroism is used to investigate the solution equilibria involving the competing ligands and to derive a spectroscopic series for Yb.

Introduction

The Schiff bases obtained in a template 2 + 2 condensation of diamines and 2,6-diformylpyridine or 2,6-diacetylpyridine are particularly suitable for the coordination of relatively large lanthanide(III) ions.[1] When the chiral precursor, *R*,*R*′-1,2-diaminocyclohexane, is used in this template reaction, chiral lanthanide(III) complexes $[Ln\mathbf{L}(NO_3)_2](NO_3)\cdot nH_2O$ and $[Ln\mathbf{L}Cl_3]\cdot nH_2O$ (where Ln is the lanthanide(III) ion and **L** the ligand of Figure 1)[2] are formed.[3−6] The coordination of a lanthanide(III) ion in a chiral macrocyclic environment leads to interesting properties of these compounds. Thus the $[Tb\mathbf{L}(NO_3)_2](NO_3)$ and $[Eu\mathbf{L}(NO_3)_2](NO_3)$ complexes were shown to exhibit circularly polarized luminescence[3] and the paramagnetic $[Eu\mathbf{L}(NO_3)_2](NO_3)$ and $[Yb\mathbf{L}(NO_3)_2](NO_3)$ complexes were shown to form diastereomeric complexes with D- and L-amino acids.[4] We have previously shown that the nitrate derivatives $[Ln\mathbf{L}(NO_3)_2](NO_3)\cdot nH_2O$ exhibit D_2-symmetry both in solution and in the solid state.[4,5] This symmetry arises from the presence of the helically twisted macrocycle and the symmetric coordination of nitrate anions above and below the macrocycle. In contrast, the X-ray crystal structures of $[Ln\mathit{rac}\mathbf{L}Cl_3]$[6a] and $[\{Yb(OH)Cl_2$-

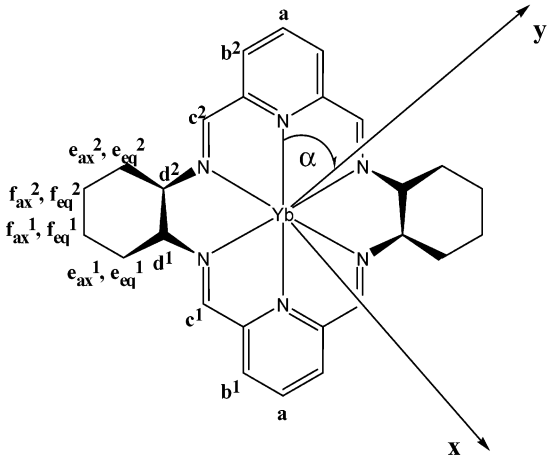

Figure 1. Structure and hydrogen labeling of the macrocyclic complex of Yb^{+3}. The Cartesian axis system is also reported; the *z*-axis is perpendicular to the nitrogen plane.

* Authors to whom correspondence should be addressed. J.L.: jurekl@wchuwr.chem.uni.wroc.pl (e-mail). L.D.B.: ldb@dcci.unipi.it (e-mail); +39 050 2219298 (tel); +39 050 2219260 (fax).

† University of Wrocław.

‡ Università di Pisa.

(1) (a) Alexander, V. *Chem. Rev.* **1995**, *95*, 273−342. (b) Aspinall, H. C. *Chem. Rev.* **2002**, *102*, 1807−1850. (c) Backer-Dirks, J. D. J.; Gray, C. J.; Hart, F. A.; Hursthouse, M. B.; Schoop, C. *J. Chem. Soc., Chem. Commun.* **1979**, 774−775.

(2) Lanthanide: Ln. 4(*R*),9(*R*),19(*R*),24(*R*)-3,10,18,25,31,35-Hexaazapentacyclo[25.3.1.1^{12,24}.0^{4,9}.0^{19,24}]dotriaconta-1(31),2,10,12,14,16(32),17,25,27,29-decaene: **L**. Sodium acetate: AcONa. Diphenyl phosphate sodium salt: DPPNa. Phenyl phosphate disodium salt: $PPNa_2$. Diphenyl phosphate acid: DPPH. Benzenesulfonic acid sodium salt: $PhSO_3Na$. The formulas $[Ln\mathbf{L}Cl_3]$ and $[Ln\mathbf{L}(NO_3)_2](NO_3)$ are used according to X-ray structures.

(3) Tsubomura, T.; Yasaku, K.; Sato, T.; Morita, M. *Inorg. Chem.* **1992**, *31*, 447−450.

(4) Lisowski, J. *Magn. Reson. Chem.* **1999**, *37*, 287−294.

(5) Lisowski, J.; Starynowicz, P. *Polyhedron* **2000**, *19*, 465−469.

(6) (a) Lisowski, J.; Mazurek, J. *Polyhedron* **2002**, *21*, 811−816. (b) Lisowski, J.; Starynowicz, P. *Inorg. Chem. Commun.* **2003**, *6*, 593−597.

10.1021/ic0353918 CCC: $27.50
Published on Web 01/27/2004

(*rac***L**)}$_2$][6b] show lower (approximate C_2) symmetry due to unsymmetrical coordination of anions above and below the macrocycle plane and to an accompanying slight bending of the macrocycle.

In paramagnetic metal complexes the observed nucleus experiences an additional shift, called the hyperfine shift (δ_{hyp}), that arises from the interaction of the nuclear and electronic spins.[7] The hyperfine shift can be separated into a through-space contribution, the pseudocontact shift (δ_{PC}), and a through-bond term, the contact shift (δ_{con}).

$$\delta_{hyp} = \delta_{PC} + \delta_{con} \quad (1)$$

The pseudocontact shift is given by the equation[7]

$$\delta_{PC} = D_1\left(\frac{1 - 3\cos^2\theta}{r^3}\right) + D_2\left(\frac{\sin^2\theta\cos 2\alpha}{r^3}\right) \quad (2)$$

where D_1 and D_2 depend on the principal components of anisotropic magnetic susceptibility tensor χ_{xx}, χ_{yy}, and χ_{zz} ($D_1 = \chi_{zz} - {}^1/_2(\chi_{xx} + \chi_{yy})$; $D_2 = {}^3/_2(\chi_{xx} - \chi_{yy})$);[7] r, θ, and α are the polar coordinates of the given nucleus, with respect to the principal axes of this tensor.

In the case of the trivalent ytterbium ion, on which the attention of this work was concentrated, the hyperfine shift derives essentially from the pseudocontact term and the contact one can be neglected. As a result, from the analysis of paramagnetic shifts by means of eq 2, the structure of ytterbium complexes can be determined.

The Yb^{+3} ion has a magnetically allowed electronic transition between the states $^2F_{7/2}$ and $^2F_{5/2}$,[8,9] split into 4 and 3 nondegenerate levels by a ligand field. The energy center of gravity of the 12 intralevel transitions is practically independent of the ligand, and it falls at 10200 cm^{-1} (980 nm), in the near-infrared (NIR) spectroscopic region. Owing to the coordination of the cation by chiral ligands, it is possible to detect NIR circular dichroism (NIR CD) bands with high dissymmetry factors.[8]

The investigation through NIR CD is particularly advantageous for manifold studies of chiral ytterbium complexes. In fact, most organic ligands are transparent in the NIR, generating no interference with the detection of ytterbium bands, and the matrix effects are eliminated; therefore by means of NIR CD of Yb^{+3} it is possible to identify unequivocally the formation of chiral adducts in solution.[10−12] Furthermore, with this spectroscopy it is possible to extract information about the absolute configuration of the ligands[11] and to investigate the chiroptical properties of the ytterbium ion.[13] NIR CD was also demonstrated to be very sensitive to the axial ligand, which is particularly relevant for the present study.[14]

Experimental Section

[Yb**L**$(NO_3)_2$](NO_3) was synthesized as described in the literature.[4] The new [Yb**L**Cl_3]·$2H_2O$ complex was prepared in the same way as [Eu**L**Cl_3]·$2H_2O$ in 60% yield.[5]

The axial ligand exchange experiments were run in NMR tubes by titrating the starting chloride or nitrate derivatives (CD_3OD or $CD_3OD/CDCl_3$ 1:2 and 1:1 v/v solutions) with the appropriate anions, which were added as the CD_3OD solutions of the sodium or lithium salts using Hamilton microsyringes. The formation of new complexes was monitored using ^1H NMR and 2D NMR measurements.

Similar titrations were followed by NIR CD spectroscopy. Stock salt solutions (see note 2 for the abbreviations) of AcONa and of $PhSO_3Na$ in $CHCl_3/CH_3OH$ 1:1, and of $PPNa_2$ in CH_3OH were prepared; detailed concentration data are reported in the figure captions. DPPNa, 24.68 mM, was prepared by reacting 7.7 μmol of DPPH in 250 μL of $CHCl_3/CH_3OH$ 2:1 with 62 μL of methanolic NaOH, 123 mM (obtained from standardized aqueous NaOH 246 mM). Different aliquots of DPPNa were added to 500 μL of [Yb**L**Cl_3]·$2H_2O$ or [Yb**L**$(NO_3)_2$](NO_3) in $CHCl_3/CH_3OH$ 2:1 up to 3−4 equiv. To determine the relative anion strength, 30 μL of AcONa was added to the mixtures Yb**L**Cl_3/$PPNa_2$ and [Yb**L**$(NO_3)_2$]$^-$ (NO_3)/$PhSO_3Na$ obtaining the systems Yb**L**Cl_3/$PPNa_2$/AcONa 1:4:3 and [Yb**L**$(NO_3)_2$](NO_3)/$PhSO_3Na$/AcONa 1:3:4.

The NMR spectra were recorded on Bruker AMX 300 and Avance 500 spectrometers. The chemical shifts were referenced to the residual solvent signal or to TMS. The magnitude COSY spectra were acquired using 1K × 512 data points. The data were processed by using a square sine bell window in both dimensions and zero filled to a 1K × 1K matrix. The EXSY spectra were recorded using standard phase-sensitive (TPPI) NOESY experiment with mixing times varying from 3 to 400 ms. HMQC spectra were recorded using BIRD preparation period and 512 × 512 data points. A square sine function was used for apodization in both dimensions. The NIR CD spectra of Yb(III) were detected on a Jasco J200D spectropolarimeter, operating between 750 and 1350 nm, modified by a tandem detector Si/InGaAs with dual photomultiplier amplifier[15] and using a 1 cm "semimicro" quartz cell. If not specified, the spectra were acquired at room temperature and then normalized to the total concentration of Yb^{+3}. The low-temperature spectra were recorded on thermostatic conditions (±2 K). Typical acquiring conditions: scan speed 50 nm/min; time constant 0.5 s; bandwidth 3.2−4.0 nm; 8−16 were averaged; sensitivity 2−5 mdeg/cm.

The [La*rac***L**Cl_3]·$3H_2O$ complex[5] was taken as a diamagnetic reference compound for the calculation of hyperfine shifts. The hyperfine shifts were the experimental constraints for a least-squares

(7) For NMR of paramagnetic complexes see: (a) La Mar, G. N.; Horrocks, W. DeW., Jr.; Holm, R. H. *NMR of Paramagnetic Molecules*; Academic Press: New York, 1973. (b) Bertini, I.; Luchinat, C. *NMR of Paramagnetic Molecules in Biological Systems*; Benjamin/Cummings: Menlo Park, CA, 1986. (c) Sherry, A. D.; Geraldes, C. F. G. C. In *Lanthanide Probes in Life, Chemical and Earth Sciences. Theory and Practice;* Bunzli, J.-C. G., Ed.; Elsevier: Amsterdam, 1989; Chapter 4. (d) Bertini, I.; Turano, P.; Vila, A. J. *Chem. Rev.* **1993**, *93*, 2833−2932. (e) Bertini, I.; Luchinat, C. *Coord. Chem. Rev.* **1996**, *150*, 1. (f) Peters, J. A.; Huskens, J.; Raber, D. J. *Prog. Nucl. Magn. Reson. Spectrosc.* **1996**, *28*, 283−350. (g) Kemple, M. D.; Ray, B. D.; Lipkowitz, K. B.; Prendergast, F. G.; Rao, B. D. N. *J. Am. Chem. Soc.* **1988**, *110*, 8275−8287.

(8) Richardson, F. S. *Inorg. Chem.* **1980**, *19*, 2806−2812.

(9) Hüfner, S. *Optical Spectra of Transparent Rare Earth Compounds*; Academic Press: New York, 1978.

(10) Di Bari, L.; Pintacuda, G.; Ripoli, S.; Salvadori, P. *Magn. Reson. Chem.* **2002**, *40*, 396−405.

(11) Di Bari, L.; Lelli, M.; Pintacuda, G.; Salvadori, P. *Chirality* **2002**, *14*, 265−273.

(12) Di Bari, L.; Lelli, M.; Pintacuda, G.; Pescitelli, G.; Marchetti, F.; Salvadori, P. *J. Am. Chem. Soc.* **2003**, *125*, 5549−5558.

(13) Di Bari, L.; Pintacuda, G.; Salvadori, P. *J. Am. Chem. Soc.* **2000**, *122*, 5557−5562.

(14) Di Bari, L.; Pintacuda, G.; Salvadori, P.; Dickins, R. S.; Parker, D. *J. Am. Chem. Soc.* **2000**, *122*, 9257−9264.

(15) Castiglioni, E. *Book of Abstracts, 6th International Conference on CD page 69*; Salvadori, P., Ed.; Vigo Cursi: Pisa, September 1997.

Scheme 1. Axial Ligand Exchange Equilibria[a]

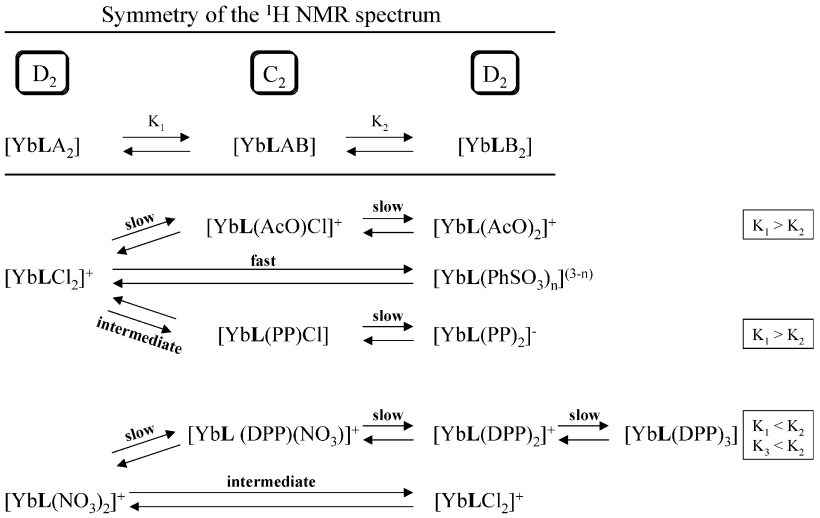

[a] Only in the case of [Yb**L**(DPP)$_3$] (C_2-symmetry) a third equilibrium was found.

fit of D_1 and D_2 and of the angle α (Figure 1), following eq 2. The optimization was accomplished by minimizing the agreement factor: $R = [\sum(\delta^{obs}_{PC} - \delta^{calc}_{PC})^2/\sum(\delta^{obs}_{PC})^2]^{1/2}$, using Mathcad 2001 and Microsoft Excel as the platform for calculations.

In an independent set of calculations, the parameters describing the paramagnetism of the ytterbium complexes (the full magnetic anisotropy susceptibility tensor) were determined by means of the program PERSEUS (Paramagnetic Enhanced Relaxation and Shifts for Eliciting Ultimate Structures).[10,12] In this case, neither the location of Yb^{+3} nor the directions of the principal axes of the anisotropy tensor were constrained a priori. By imposing equal pseudocontact shifts (δ_{PC}) for symmetry-related protons, a symmetric tensor (and therefore effective symmetry axes) was retrieved a posteriori.

Results and Discussion

Exchange of Axial Ligands. The $[Yb\mathbf{L}]^{+3}$ complexes with different axial ligands were studied by displacing an anion with a different one in titration experiments. The starting compounds were $[Yb\mathbf{L}(NO_3)_2](NO_3)$ and $[Yb\mathbf{L}Cl_3]\cdot 2H_2O$, which were synthesized using $Yb(NO_3)_3$ or $YbCl_3$ as the source of the rare earth ion. The following axial anions were used: acetate (AcO^-), diphenyl phosphate (DPP^-), phenyl phosphate (PP^{-2}), and benzenesulfonate ($PhSO_3^-$). The process of ligand exchange was followed by means of ^{1}H NMR and NIR CD spectroscopies.

As we shall further discuss below, the variation of axial ligand apparently does not alter the macrocycle conformation; thus all the ^{1}H NMR spectra can be fully accounted for by the solid state structure of $[Tm\mathbf{L}(NO_3)_2](NO_3)$. However, we can expect a very remarkable influence on the magnetic susceptibility tensor and on the shape and intensity of the NIR CD spectrum. As already demonstrated in several instances,[14,16−18] both spectroscopic data rely upon the crystal field parameters, which in turn are determined by the nature and the spacial arrangement of charged and polarizable groups around the metal ion, thus on the axial ligands.

During the course of the titration, where the axial ligand **A** is displaced by **B**, two steps can be envisaged.

$$Yb\mathbf{LA}_2 \overset{K_1}{\rightleftharpoons} Yb\mathbf{LAB} \overset{K_1}{\rightleftharpoons} Yb\mathbf{LB}_2$$

Therefore, species of different symmetry can be expected: the first and the last have a D_2-symmetry, and the intermediate species is C_2. This is immediately recognized by the number of proton resonances: 8 shifts are predicted for Yb**LA**$_2$ and Yb**LB**$_2$, 15 shifts for Yb**LAB**.

In most cases, the exchange processes can appear slow on the ^{1}H NMR time scale with the uprise of the new species taking place at the same time with the disappearing of the previous one during the course of the titration. Sometimes, a typical intermediate exchange is observed, with extensive line broadening until one of the forms dominates (i.e. at the beginning and at the end). The results are summarized in Scheme 1.The stoichiometries indicated in Scheme 1 cannot be considered fully definitive, since the further ion needed for the electroneutrality of the species cannot be safely determined (moreover it may or may not be involved in a tight ion pair, considering the high polarity of the solvent used).

The relative values of the two formation constants determine which species can coexist: only if $K_2 \geq K_1$ the third complex can be formed in substantial concentrations at [**B**]/[**A**] < 1. In turn, the relative strengths of the two competing axial ligands determine through K_1K_2 if the third complex is formed after adding 2 equiv of the titrating anion or only after adding a large excess of the titrating anion. The latter is the case for $[Yb\mathbf{L}(NO_3)_2]^+ \rightarrow [Yb\mathbf{L}Cl_2]^+$, a reaction which is not complete even in the presence of a 10-fold excess of Cl^-, and which occurs at an intermediate exchange rate. This result is consistent with weaker binding properties of chloride in comparison to nitrate anion.

In the case of the titration of $[Yb\mathbf{L}Cl_2]^+$ complex with $PhSO_3^-$ the axial ligand exchange is fast on the NMR time

(16) Bleaney, B. *J. Magn. Reson.* **1972**, *8*, 91−100.
(17) (a) Mironov, V. S.; Galayametdinov, Y. G. *J. Chem. Phys.* **2002**, *116*, 4673−4685. (b) Mironov, V. S.; Galayametdinov, Y. G.; Ceulemans, A.; Goerller-Walrand, C.; Binnemans, K. *Chem. Phys. Lett.* **2001**, *345*, 132−140.
(18) (a) Lisowski, J.; Sessler, J. L.; Lynch, V.; Mody, T. D. *J. Am. Chem. Soc.* **1995**, *117*, 2273−2285. (b) Lisowski, J.; Sessler, J. L.; Mody, T. D. *Inorg. Chem.* **1995**, *34*, 4336−4342.

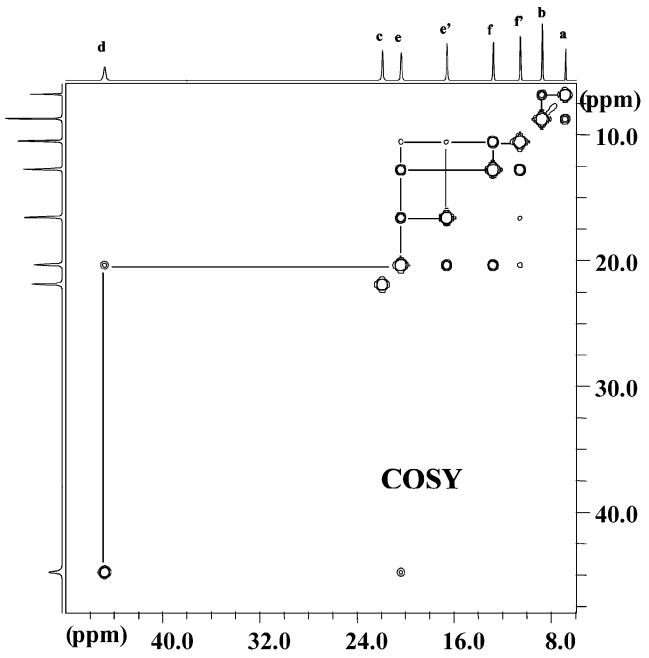

Figure 2. COSY spectrum of $[Yb\mathbf{L}(AcO)_2]^+$.

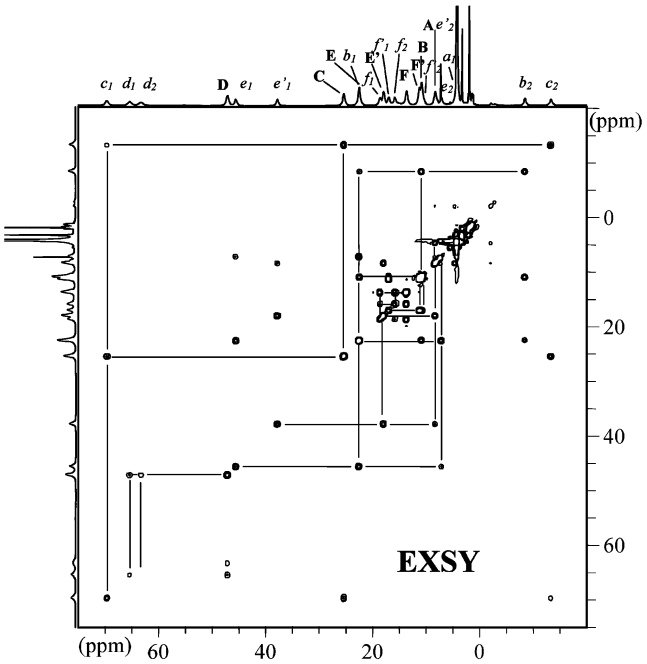

Figure 3. EXSY spectrum of the system $[Yb\mathbf{L}Cl(AcO)]^+/[YbL(AcO)_2]^+$; capital letters indicate the signals of the second species.

scale and averaged shifts of the chloride and benzenesulfonate derivatives are observed; therefore no indication for the stoichiometry of this species is given.

Assignment of the NMR Spectra. The ^{1}H NMR spectrum of the $[Yb\mathbf{L}(NO_3)_2]^+$ complex has been assigned previously[4] on the basis of 2D NMR measurements. The signals of the $[Yb\mathbf{L}(AcO)_2]^+$ and $[Yb\mathbf{L}(PP)_2]^-$ complexes, generated in solution, were assigned similarly on the basis of COSY, NOESY, and HMQC data. The HMQC spectrum of $[Yb\mathbf{L}(AcO)_2]^+$ complex identifies the two pairs of geminal protons e_{ax}, e_{eq} and f_{ax}, f_{eq} (see Figure 1 for the labeling scheme) that are correlated to one ^{13}C signal each. These signals are also correlated in the COSY spectrum (Figure 2). Additionally, one of these geminal protons, namely, e_{ax}, is COSY correlated to another signal that must correspond to d. Similarly, the signals of f_{ax} and f_{eq} can be distinguished on the basis of the observed COSY correlation between the signals e_{ax} and f_{ax}. The COSY spectrum additionally shows the correlated pair of the protons a and b, while the signal of the proton c exhibits no COSY correlations. The above assignment can be confirmed on the basis of the NOESY spectrum that can be followed conveniently starting from the easily identified (on the basis of integration) signal of the proton a. An identical assignment can be made for the $[Yb\mathbf{L}(PP)_2]^-$ complex.

Severe line broadening prevents the assignment of $[Yb\mathbf{L}Cl_2]^+$ through correlation techniques. Favorable dynamic rates, instead, allowed us to use EXSY (Figure 3) on the exchange:

$$[Yb\mathbf{L}Cl_2]^+ \overset{\text{slow}}{\rightleftharpoons} [Yb\mathbf{L}Cl(AcO)]^+ \overset{\text{slow}}{\rightleftharpoons} [Yb\mathbf{L}(AcO)_2]$$

Thus the full knowledge of the latter complex resolved the assignment of the first one as well.

Similar EXSY spectra are measured for the mixtures of those complexes, that have slow exchange rates on the NMR time scale, as summarized in Scheme 1, completing the resonance assignment. Interestingly, EXSY spectra show not only intermolecular but also intramolecular cross-peaks, that correlate different signals within the same complex of C_2-symmetry (Figure 3). This latter correlation arises from two subsequent ligand exchange reactions that interchange the top and bottom of the macrocycle, thus switching positions of two-quarters of the macrocycle, e.g., pyridine positions b^1 and b^2 (Figure 4).

It must be noticed that line broadening of the $[Yb\mathbf{L}Cl_2]^+$ signals was ascribed to an additional exchange process. In fact, stepwise addition of LiCl into a CD_3OD solution of $[Yb\mathbf{L}Cl_3]\cdot 2H_2O$ results in some narrowing of the lines, indicating that this complex is involved in an exchange. This dynamics can be slowed down at lower temperature (203−330 K). Although the low temperature spectra are rather complicated and cannot be fully assigned due to line broadening and overlap, an increase of the number of the resonances is observed below 270 K. This clearly indicates the presence of lower symmetry species. Additionally, EXSY correlations between signals of $[Yb\mathbf{L}Cl_2]^+$ measured at 223 K confirm the presence of a dynamic exchange of the chloride ligands.

Analysis of Pseudocontact Shifts. In the case of the ytterbium(III) complexes with the ligand **L** it can be expected that the shifts are dominated by the pseudocontact shift contribution.[7e] Any change in the observed spectrum may in principle result from two mechanisms: the change of the macrocycle geometry or the change of the principal values and/or directions of the magnetic susceptibility tensor of the complex, that reflects upon the D_1 and D_2 values. The X-ray crystal structures of the various lanthanide(III) complexes of the ligand **L** show some flexibility of this ligand, but the overall geometry of **L** is not very different in each case. Consequently the second mechanism appeared responsible

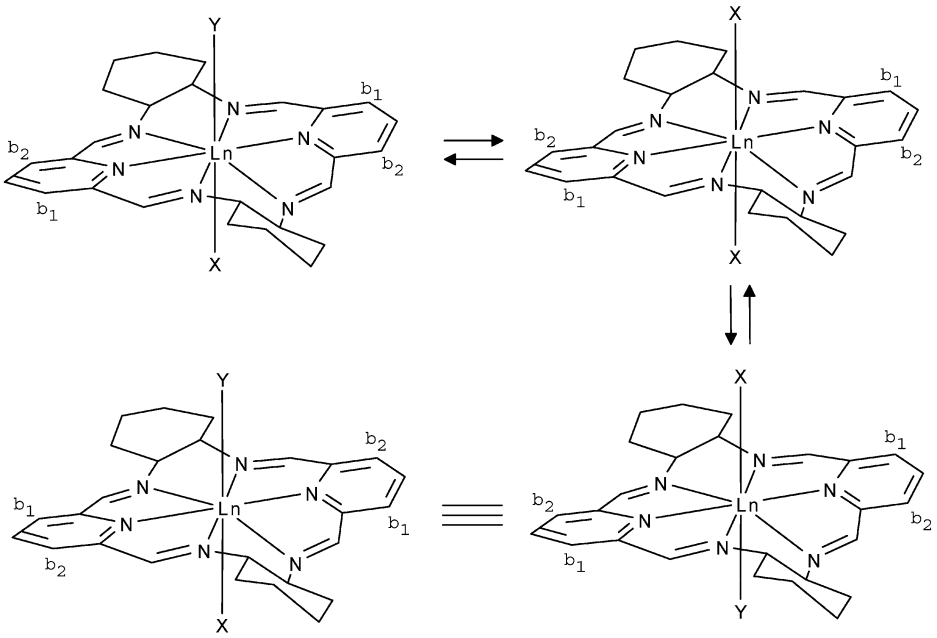

Figure 4. Exchange dynamics in solution.

for most of the changes in the lanthanide-induced shifts. Similar dramatic changes of pseudocontact shifts caused by the exchange of axial ligands (accompanied by the change of crystal field parameters)[16,17] have been observed in the case of lanthanide(III) texaphyrins[18] and of DOTA derivatives.[14]

We were actually able to fit the data for all the complexes with the same geometry, taken from the X-ray structure of [Tm**L**$(NO_3)_2$]$(NO_3)\cdot CH_3OH$.[5] In the case of D_2-symmetry, only D_1 and D_2 need to be determined, since the directions of the principal axes of the magnetic susceptibility tensor must be along the symmetry axes. For the lower symmetry cases the only C_2-axis coincides with one of the tensor axes. This fact is accounted for by α, which we define as the angle between the line joining the two pyridine nitrogens and the principal axis lying on the macrocycle plane. Hence the parameters D_1 and D_2 as well as the angle α must be determined.

It must be noticed that in the case of a fast or intermediate exchange between two adducts with different axial ligands (**A** and **B**), the observed pseudocontact for the *i*th nucleus can be written as

$$\delta^{PC}_{obs,i} = \sum_j D^j_A G^j_A x_A + \sum_j D^j_B G^j_B x_B \qquad (3)$$

where x_A and x_B are the molar fractions of the two complexes; G^j_A and G^j_B are the geometrical factors with $j = 1, 2$ that indicates the two terms in which the δ^{PC} is factorized. Considering the rigidity of the macrocycle **L**, and assuming a constant orientation of the principal axes (which is true by necessity for the D_2-symmetric cases), the identity of the geometrical factors follows ($G^1_A = G^1_B = G_1$ and $G^2_A = G^2_B = G_2$) so that eq 3 reduces to $\delta^{PC}_{obs,i} = D_1G_1 + D_2G_2$, where D_1 and D_2 are *phenomenological* parameters given by $D_j = D^j_A x_A + D^j_B x_B$, thus mixing up information from both axially ligated species.

To determine the magnetic parameters of Yb^{+3}, the ^1H NMR shifts of the complexes of Scheme 1 were analyzed by means of two different calculations.

(I) For all the complexes featuring D_2-symmetry, the principal components of the anisotropy tensor must be found along the three C_2-axes of the X-ray structure of [Tm**L**$(NO_3)_2$]$^+$. Consequently, defining as *z* the axis perpendicular to the plane of the six nitrogen atoms and *y* that along the Yb^{+3}/pyridine bond, the geometric factors of eq 2 are defined (in this case $\alpha = 0$). D_1 and D_2 can be treated as fitting parameters and varied to obtain the best agreement between calculated and experimental pseudocontact shifts.[19] In the case of the complexes having ^1H NMR compatible with lower symmetry, only the C_2-axis perpendicular to the plane is conserved, and it is chosen as the *z*-axis, while *x* and *y* cannot be a priori deduced. In this case, the angle α describes the rotation of *y* with respect to the Yb^{+3}/pyridine direction chosen above (Figure 1), and it must be optimized, as well.

(II) Using the program PERSEUS[10,12] on the same X-ray set of coordinates, one can treat the location of Yb^{+3} and the whole magnetic susceptibility anisotropy tensor (orientation of the principal system and its principal values) as fitting parameters. Coincidence between inertial and magnetic axes for the D_2-symmetric system is thus retrieved a posteriori, as well as the distance between the X-ray position of Tm^{+3} and the optimized location of Yb^{+3} (this distance is below 0.3 Å).

The results are summarized in Tables 1 and 2. Both calculations yield a good reproduction of the pseudocontact shifts (the agreement factors are in the range 3.6−11.4%). The fitted principal values of the anisotropy tensor (or the derived quantities D_1 and D_2) are in excellent agreement (well

(19) Naturally, by a different choice of the *z* and *y* axes, different geometric factors are calculated and new sets of D_1 and D_2 are found, accordingly.

Table 1. Complexes with a NMR Spectrum of D_2-Symmetry: Calculated Values of D_1 and D_2 (ppm × Å^3, Error within 10−20%) (Fitting I) and of the Components of the Magnetic Susceptibility Tensor (Program PERSEUS) in Its Principal Axis System (*a*, *b*, *c*) of Figure 5a[a]

	$[YbLCl_2]^+$	$[YbL(NO_3)_2]^+$	$[YbL(AcO_2)]^+$	$[YbL(PP)_2]^-$	$[YbL(DPP)_2]^+$	$[YbL(PhSO_3)_n]^{3-n}$
D_1	-440	-400	1580	3900	2250	440
D_2	3020	1690	1930	3870	5100	3670
χ_a'	-860	- 420	-1170	-2560	-2450	-1370
χ_b'	-290	-260	1060	2620	1520	290
χ_c'	1150	690	110	-30	920	1080

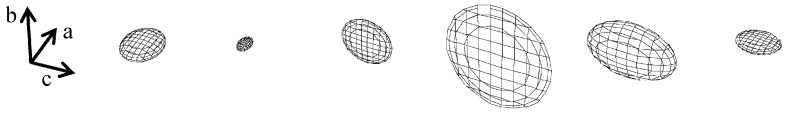

[a] In the bottom line, the magnetic susceptibility ellipsoids generated by the three components are also depicted.

Table 2. Complexes with a NMR Spectrum of C_2-Symmetry: Calculated Values of D_1, D_2 (ppm × Å^3, Error within 10−20%), and α (deg, ±5°) (Fitting I) and of the Components of the Magnetic Susceptibility Tensor (Program PERSEUS) in Its Principal Axis System (*a*, *b*, *c*) of Figure 5b[a]

	$[YbL(AcO)Cl]^+$	$[YbL(PP)Cl]$	$[YbL(DPP)(NO_3)]^+$	$[YbL(DPP)_3]$
D_1	1650	3060	1900	3000
D_2	-4870	-6350	-4010	-7510
α	64	61	68	70
χ_a'	1080[i]	1080	700	1500
χ_b'	1080[i]	2040	1250	1950
χ_c'	-2160[i]	-3120	-1950	-3450

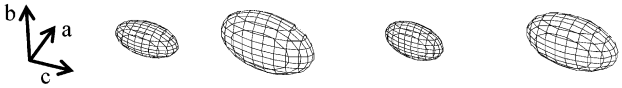

[a] In the bottom line, the magnetic susceptibility ellipsoids are also depicted. Superscript i designates that C_2-symmetry was imposed.

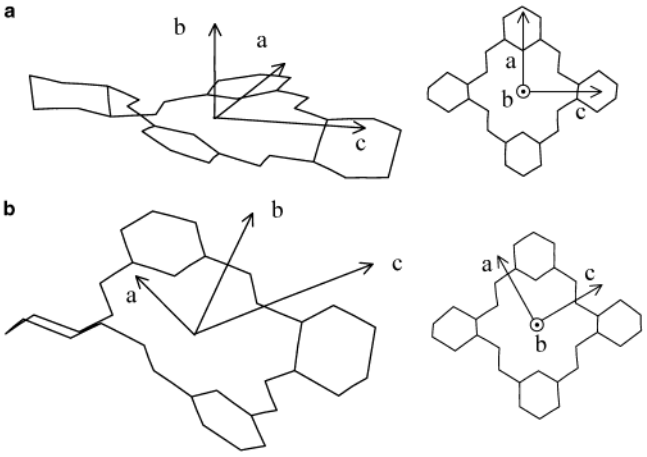

Figure 5. Projection of the structure of the macrocycle **L** (for clarity the hydrogen atoms are not shown) and the orientation of the molecular frame axes (*a*, *b*, *c*) along which the principal axes of the susceptibility tensor are directed (Tables 1 and 2); Yb^{+3} is located in the origin. (a) Representation relative to the complexes with a NMR spectrum of D_2-symmetry: with respect to the Yb−N_{Py} axis the average orientation of (*a*, *b*, *c*) is (2°, 89°, 90°), respectively. (b) Representation relative to the complexes with a NMR spectrum of C_2-symmetry: with respect to the Yb−N_{Py} axis the average orientation of (*a*, *b*, *c*) is (24°, 94°, 66°), respectively.

within the error), demonstrating the equivalence of the two independent methods. Also the angle α is similarly determined for C_2-symmetric complexes, where one of the two in-plane axes is found practically directed along the Yb^{+3}/imine−nitrogen bond (Figure 5). The spread of the anisotropy tensor principal values is very large and indicates a heavy influence of the axial binding. Accordingly, the tensor can assume very different shapes from discoid to bar-like (Tables 1 and 2).

Similar results of calculations were also obtained using the coordinates of $[Gd\mathbf{L}(H_2O)_3]Cl_3 \cdot 3H_2O$ complex[20] or MM2 modeled structure of the Yb(III) complex.[21] The 10−20% differences of the D_1, D_2 and the axis directions reflect the accuracy of the calculations and indicate the magnitude of the contributions arising from the slightly different geometry of the macrocycle **L** in different axial ligand derivatives. The results clearly support the assumption that minor changes of geometrical positions accompanying the change of axial ligands are not the primary cause of the observed dramatic changes of chemical shifts, and conversely, on the basis of these data one cannot ascertain if the macrocycle itself changes its symmetry from D_2 to C_2. Thus the starting X-ray structure of the complex can be considered a good solution model.

The extension of conjugation, characterizing the ligand, might transfer the contact effect (difficult to estimate) also to a proton more distant than three bonds from Yb^{+3}; this might be the reason for the less accurate fitting than for other systems.[12,22]

NIR CD Analysis. The chiral complex $[Yb\mathbf{L}Cl_3] \cdot 2H_2O$ has a spare solubility in $CHCl_3$, which however allows the detection of its NIR CD spectrum, characterized by a single positive band centered about on 980 nm. The addition of 0.5 equiv of methanol to this sample produces a very different spectrum, characterized by a dissignated doublet: a positive band at 982 nm and a negative one at 976 nm, with the same intensity (see Supporting Information). The shape of the latter spectrum is identical to that relative to a solution of $[Yb\mathbf{L}Cl_3] \cdot 2H_2O$ in the solvent mixture $CHCl_3/CH_3OH$ 2:1 (Figure 6a); this spectrum is characterized by two bands with opposite sign, originated by at least three f−f transitions, as shown by the low temperature spectrum (see Supporting Information). The dramatic changes of the spectrum after adding methanol may be justified by the involvement of methanol in the coordination sphere; however, its location

(20) Bligh, S. W. A.; Choi, N.; Cummins, W. J.; Evagorou, E. G.; Kelly, J. D.; McPartlin, M. *J. Chem. Soc., Dalton Trans.* **1994**, 3369−3376.
(21) Also in the case of the unsymmetrical structure of [{Yb(OH)Cl_2-(*rac***L**)}$_2$] equivalent solutions were found.
(22) Di Bari, L.; Pintacuda, G.; Salvadori, P. *Eur. J. Inorg. Chem.* **2000**, 75−82.

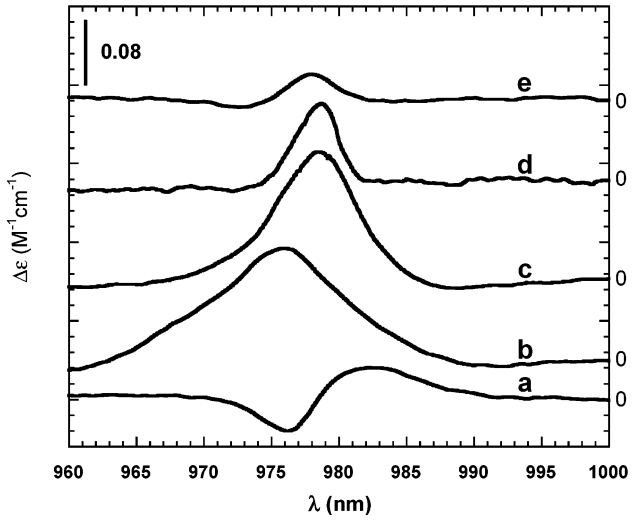

Figure 6. NIR CD spectrum of (a) [Yb**L**Cl_3]·$2H_2O$ (6.52 mM) in $CHCl_3$/MeOH 2:1; (b) [Yb**L**$(NO_3)_2(NO_3)$] 6.10 mM in $CHCl_3$/MeOH 2:1; (c) [Yb**L**$(NO_3)_2(NO_3)$] 3.13 mM in $CHCl_3$/MeOH 2:1 after addition of 2.4 equiv of AcONa (130.00 mM); (d) [Yb**L**Cl_3] 2.67 mM in $CHCl_3$/MeOH 2:1 after addition of 3.5 equiv of $PPNa_2$ (57.47 mM); (e) [Yb**L**$(NO_3)_2(NO_3)$] 3.50 mM in $CHCl_3$/MeOH 2:1 after addition of 2.5 equiv of DPPNa (24.68 mM).

in the inner/outer sphere is not straightforward. Nevertheless, these results allow us to clarify further the solution dynamics of the [Yb**L**Cl_2]$^+$ complex above noticed and that of the family of complexes Ln**L**Cl_3 recently found by NMR spectroscopy.[6a] The direct participation of methanol in the coordination of the metal cation may indicate that in the solution equilibria, nominally between Yb**L**Cl_3 and [Yb**L**Cl_2]$^+$,[6a] species involving the solvent may play a role.

The spectrum of a solution of [Yb**L**$(NO_3)_2$](NO_3), shown in Figure 6b, is very different from that of the chloride derivative: it is characterized by a very large and positive band at 976 nm, which resolves into three components at 223 K (see Supporting Information).

The titration of [Yb**L**Cl_3]·$2H_2O$ with AcONa leads to a final spectrum characterized by a relatively large and positive band at 978 nm, already evident starting from the addition of 0.5 equiv of acetate (Figure 6c). Similarly, the stepwise adding of $PPNa_2$ produces a relatively sharp and positive band at 979 nm starting from 0.5 equiv of PP^{-2} (Figure 6d). Performing a titration of the nitrate derivative with DPPNa, the spectrum of the complex passes from that assignable to [Yb**L**$(NO_3)_2$]$^+$ to one with a sharper positive band at 978 nm and a very weak negative band at 973 nm (Figure 6e).

The addition of $PhSO_3Na$ to a [Yb**L**Cl_3]·$2H_2O$ solution does not determine modifications either of the intensity or of the band shape. By a similar titration of **[YbL**$(NO_3)_2$]$^+$ one observes a progressive decrease of the intensity of the complex band without changes of shape.

The spectra of all species can be divided into two groups: the first one is characterized by a single positive band, ascribable to the presence of anions in the inner coordination sphere of Yb^{+3}; the second kind shows a dissignate doublet and may be associated to the involvement of methanol.

Furthermore, some information about the relative coordinating strength of the anions was deduced through cross anion exchanges. Because the addition of $PhSO_3^-$ both to [Yb**L**$(NO_3)_2$]$^+$ and [Yb**L**Cl_2]$^+$ does not substantially change their spectra, this anion can be considered the weakest one; DPP^- instead replaces the NO_3^- ion, with which the methanol does not compete. The AcO^- and PP^{2-} ions are undoubtedly stronger than methanol and chloride, and presumably the PP^{-2} has a strength comparable with that of DPP^-, whereas the AcO^- is weaker than PP^{-2} (adding AcONa to [Yb**L**$(PP)_2$]$^-$, the intensity and shape of its NIR CD band does not change) but it substitutes the nitrate anion; so the following series is suggested:[23]

$$PhSO_3^- < Cl^- < NO_3^- < AcO^- < PP^{-2}, DPP^-$$

Conclusions

Consistent calculation results of very different sets of dipolar shifts were obtained for various Yb(III) derivatives using one structure of the macrocycle: the observed dramatic influence of axial ligands on NMR spectra is encoded only into the magnetic anisotropy parameters. Importantly, the calculated parameters explain the striking difference of chemical shifts, observed for the C_2-symmetric complexes, between the two sets of signals: b^1 to f_{eq}^1 and b^2 to f_{eq}^2. This difference is a result of unprecedented rotation of the axes of the magnetic susceptibility tensor within the macrocycle plane. This rotation leads to very different psuedocontact shifts experienced by the two correspondent quarters of the macrocycle.

The macrocyclic ligand **L**, practically confined within a thin equatorial region, leaves the lanthanide exposed to donor species on both sides of a perpendicular axis. This makes the complex an ideal substrate to study the role of axial ligation to lanthanides. By the concerted use of optical and NMR spectroscopies, it was possible to characterize the relative strengths of the ligands and to provide data on the magnetic anisotropy, which in turn has an effect of the crystal field.

The impressive changes in both optical and NMR spectroscopies upon axial ligand exchange make this system promising for anion sensing in nonaqueous environment. Moreover, a variation of the lanthanide cation offers the possibility of tuning to the best suited spectroscopy (absorption, fluorescence, ...), and the presence of a stereodefined macrocycle opens the way to the enantiodiscrimination of anionic substrates.

Acknowledgment. CNR, ICCOM-sezione di Pisa, and Polish Committee for Scientific Research (KBN grant 3T09A 11519) are gratefully acknowledged for financial support.

Supporting Information Available: Experimental and calculated proton shifts; molar ratio analysis of NIR CD spectra; NIR CD spectrum of [Yb**L**Cl_3]·$2H_2O$ in $CHCl_3$; NIR CD spectra at low temperature. This material is available free of charge via the Internet at http://pubs.acs.org.

IC0353918

(23) Methanol is likely located between Cl^- and NO_3^- in the strength scale; however, it was not included in this series because its participation in the first or second coordination sphere is not completely clear.